Received: 28 August 2019 | Accepted: 31 October 2019

DOI: 10.1113/EP088133

Experimental Physiology WILEY

RESEARCH PAPER

Semi-automatic methods for tracking the medial gastrocnemius muscle–tendon junction using ultrasound: a validation study

Francesco Cenni[1,2] | Lynn Bar-On[3,4] | Davide Monari[2,5] | Simon-Henri Schless[6] | Barbara M. Kalkman[7] | Erwin Aertbeliën[5] | Kaat Desloovere[2,3] | Herman Bruyninckx[5]

[1]KU Leuven, Department of Movement Sciences, Tervuursevest 101, 3001 Leuven, Belgium

[2]Clinical Motion Analysis Laboratory, University Hospital Leuven, Weligerveld 1, 3212 Pellenberg, Belgium

[3]KU Leuven, Department of Rehabilitation Sciences, Tervuursevest 101, 3001 Leuven, Belgium

[4]Amsterdam UMC, Vrije Universiteit Amsterdam, Department of Rehabilitation Medicine, Amsterdam Movement Sciences, Amsterdam, Netherlands

[5]KU Leuven, Department of Mechanical Engineering, Celestijnenlaan 300b, 3001 Leuven, Belgium

[6]Alyn Hospital, Pediatric and Adolescent Rehabilitation Center, Jerusalem, Israel

[7]Research Institute for Sport and Exercise Sciences, Liverpool John Moores University, Liverpool, UK

Correspondence
Francesco Cenni
Email: francesco.cenni@kuleuven.be

Funding information
The authors are supported by the following funding bodies: postdoctoral mandate of the KU Leuven, Belgium (PDM/18/181); post-doctoral grant (12R4215N) and by a project grant (T005416N) from the Flemish Research Foundation (FWO), Belgium; post-doctoral grant (016.186.144) from the Dutch Research Foundation (NWO). Funding was also received from 'La Fondation Motrice', contract 2016/8. The funders had no role in investigation-design, data collection and analysis, decision to publish, or preparation of the manuscript.

Edited by: Daniel Wilkinson

Abstract

Clinically relevant information can be extracted from ultrasound (US) images by tracking the displacement of the junction between muscle and tendon. This paper validated automatic methods for tracking the location of muscle–tendon junction (MTJ) between the medial gastrocnemius and the Achilles tendon during passive slow and fast stretches, and active ankle rotations while walking on a treadmill. First, an automatic algorithm based on an optical flow approach was applied on collected US images. Second, results of the automatic algorithm were evaluated and corrected using a quality measure that indicated which critical images need to be manually corrected. US images from 12 typically developed (TD) children, 12 children with spastic cerebral palsy (SCP) and eight healthy adults were analysed. Automatic and semi-automatic tracking methods were compared to manual tracking using root mean square errors (RMSE). For the automatic tracking, RMSE was less than 3.1 mm for the slow stretch and 5.2 mm for the fast stretch, the worst case being for SCP. The tracking results in the fast stretch condition were improved (especially in SCP) by using the semi-automatic approach, with an RMSE reduction of about 30%. During walking, the semi-automatic method also reduced errors, with a final RMSE of 3.6 mm. In all cases, data processing was considerably shorter using the semi-automatic method (2 min) compared to manual tracking (20 min). A quick manual correction considerably improves tracking of the MTJ during gait and allows to achieve results suitable for further analyses. The proposed algorithm is freely available.

KEYWORDS

medial gastrocnemius, tracking, ultrasound, validation

1 | INTRODUCTION

Tracking of the muscle–tendon junction (MTJ) using ultrasound (US) during joint movement can be used to calculate muscle and tendon lengthening. This has previously been investigated for the medial gastrocnemius (MG) and Achilles tendon (AT) to compare their mechanical and functional properties (Kalsi, Fry, & Shortland, 2016; Sikdar, Wei, & Cortes, 2014; Theis, Mohagheghi, & Korff, 2016).

© 2019 The Authors. Experimental Physiology © 2019 The Physiological Society

However, manual tracking of the MTJ is time consuming. Fully automatic tracking methods have previously been proposed, although details about their performance in impulsive joint movements and in pathological populations are still lacking. In addition, a software package that also allows manual interventions in case of failure is needed.

The analysis of the MTJ behaviour involves dynamic imaging whereby an US probe is placed over the relevant anatomical region, and sequences of 2D B-mode images are recorded during joint movement. This imaging method has previously been applied for tracking the MG MTJ in children with spastic cerebral palsy (SCP) during passive ankle rotation (Bar-On et al., 2018), walking (Barber et al., 2017; Kalsi et al., 2016), calculations of tendon stiffness (Maganaris, 2002) and muscle moment arm lengths (Ito, Akima, & Fukunaga, 2000; Kalkman et al., 2017). The MTJ is identified as the landmark where the muscle meets the tendon. However, intrinsic errors for detecting this landmark using 2D US are evident (Cenni et al., 2018). Longitudinal 2D US images only allow an approximation of the MTJ 'V' shape within one plane. In addition, during joint movement, the MTJ may move out of the imaged plane (Cenni et al., 2018). Another problem, in particular for neuromuscular disorders such as in children with SCP, is the alteration of the internal composition of the muscle leading to a hyper-echoic appearance with US (Obst, Boyd, Read, & Barber, 2017; Pitcher et al., 2015; Schless et al., 2018), making the boundary between muscle and tendon less distinct. Due to this, manual tracking of the MTJ acquired during dynamic US imaging is still largely utilized as a safe solution, relying on experienced operators.

This manual procedure can be considered as an acceptable compromise when only a few US images are needed. However, in situations in which many US images require processing, a method to automatically extract the data is of great clinical utility. Previously, automated techniques that constrain the shape of the tracked features were introduced (Cronin, Carty, Barrett, & Lichtwark, 2011; Rana, Hamarneh, & Wakeling, 2009; Zhao & Zhang, 2011). Recently, more generic applications accounting for local shape changes of different muscle features have also been utilized (Darby, Hodson-Tole, Costen, & Loram, 2012, 2013). However, these applications require a training set of objects to provide a good representation of the overall distribution of allowable shapes, thereby limiting their direct clinical use for a specific pathological population. This limitation can be overcome by a number of automated methods using optical flow (OF) or template matching approaches (Lee, Lewis, & Piazza, 2008; Magnusson et al., 2003; Pearson, Ritchings, & Mohamed, 2013). These methods have potentially wider applications and can be used for muscles and tendons, as well as for different types of movement. The OF approach is defined as the pattern of motion of objects between two consecutive images, assuming that pixel intensities are translated from one image to the next. OF methods have shown satisfactory results (Lee et al., 2008; Magnusson et al., 2003; Pearson et al., 2013), albeit in small populations of healthy participants. The template matching approach is based on searching for a relevant region of interest (ROI) among the images, by means of similarity measurements. Both approaches require an image-to-image MTJ displacement that is relatively small in order to optimize the detection of the relevant pixels and ROIs in the following image. Impulsive joint movements or pathological conditions could hide or deform these features in some images, thereby triggering failure of the automatic tracking approach. Hence, tools for supervising tracking performance are needed to improve the corresponding outcome.

New Findings

- **What is the central question of this study?**
  Is the proposed semi-automatic algorithm suitable for tracking the medial gastrocnemius muscle–tendon junction in ultrasound images collected during passive and active conditions?
- **What is the main finding and its importance?**
  The validation of a method allowing efficient tracking of the muscle–tendon junction in both passive and active conditions, in healthy as well as in pathological conditions. This method was tested in common acquisition conditions and the developed software made freely available.

The objective of the present investigation was threefold. First, we aimed to describe and provide an open-source software library capable of automatically tracking the MTJ by using the OF approach. Second, we aimed to validate the application of the algorithm by tracking the MG MTJ during passive ankle rotations in cohorts of children with SCP and typically developing (TD) children, and during active rotations in healthy adults. The results defined by the automatic methods were then compared to the manually extracted results. Third, a quality measurement was developed and applied to improve the automatic tracking results. When the automatic algorithm fails, the quality measurement can support the operator in performing a manual feature extraction by indicating those images that are responsible for triggering the tracking error. This approach is referred to as a semi-automatic method. It is hypothesized that the successful automated method provides similar results to the manual method, below the intrinsic error in detecting the MTJ. In addition, we expect that the supervision and manual intervention by means of quality measurement provides clear indications on how to repair the tracking errors in cases in which the automated method is not considered entirely successful.

2 | METHODS

2.1 | Ethical approval

The study conformed with the latest revision of the *Declaration of Helsinki*, except for registration in a database. The procedures have been approved by the University Hospital ethics committee in Leuven (study number s57384) and the National Health Service ethics committee (study no. 15/LO/0856). Written informed consent was

acquired from the participants and from the parents/guardians of all participants in accordance with local regulations.

2.2 | Participants

Twelve TD children (age: 9.9 ± 2.0 years) and 12 children with SCP (age: 10.4 ± 2.3 years, 5/7 unilateral/bilateral, 6/6 with gross motor function classification system (GMFCS) I/II) were recruited for this multicentre study from the University Hospital in Leuven (Belgium) and the Alder Hey Children's Hospital in Liverpool (UK). Eight healthy adults (age: 24.9 ± 3.9 years) were also recruited at the University Hospital in Leuven.

2.3 | Data acquisition

Children lay prone on a bed with the examined limb placed in a custom-made orthotic, maintaining 20 deg knee flexion and free sagittal plane movement at the ankle. A 2D B-mode US system (Telemed EchoBlaster 128 Ext-1Z system, Lithuania) with a 59 mm linear transducer (Telemed, HL9.0/60/128Z, Lithuania) was securely placed over the MG MTJ junction, positioned along the main AT pulling direction. This direction was found by extending the MG's mid-longitudinal plane, defined by marking its origin through the muscle belly to the MTJ (Bénard, Becher, Harlaar, Huijing, & Jaspers, 2009). US images (pixel resolution of 0.1 mm) were recorded during passive ankle movements manually applied by the same operator across the full range of motion, from plantar- to dorsiflexion and vice versa. This was performed at a slow velocity (approximately 5 s over the full range of motion) and then as fast as possible (approximately 1 s over the full range of motion). This manual procedure was found to be repeatable (Bar-On et al., 2013; Schless et al., 2015). To achieve the best compromise between spatial and temporal resolution, US images during the slow velocity movement were acquired at 30 Hz, and during the fast velocity movements at 60 Hz.

Data from healthy adults were acquired while walking on a treadmill at a self-selected speed (Motek Medical; Amsterdam, the Netherlands). The same instrumentation and conventions used in the children were adapted for the adults while walking, i.e. the US probe was secured over the skin surface with a compressive bandage (Barber et al., 2017), and data were acquired at 30 Hz (Figure 1).

2.4 | The automatic tracking algorithm

The following sections describe the software features. An in-house software package (Py3DFreeHandUS, available at https://gitlab.com/u0078867/py3dfreehandus) was developed in Python 2.7 (www.python.org) to automatically track the MTJ in sequences of US images. This automatic tracking was applied using OF. Since this is an iterative process, tracking errors may accumulate over time. For this reason, a method to assist the manual intervention was implemented. The OF equation has two unknown variables. This problem can be solved by applying the Lucas–Kanade differential method between consecutive images that assumes all the neighbouring pixels around

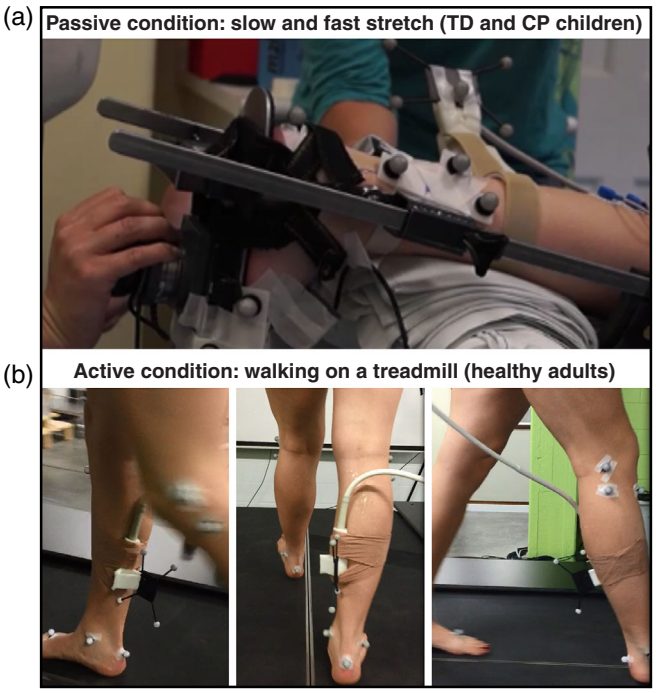

FIGURE 1 (a) The leg is positioned in a custom-made orthotic to control the manually applied slow and fast stretch at the ankle joint. The foot-plate of the orthotic is also visible. The US probe is secured over the MTJ. (b) Three views of a participant while walking on a treadmill. A bandage is used to secure the US probe. The data collected from the markers on the leg and foot were not utilized in the present investigation

the point of interest will have similar motion. A 3 × 3 patch is taken around that point to make the problem overdetermined, which is solved according to the least squares criterion (Lucas & Kanade, 1981). In order to satisfy the assumption of small motions, a pyramid representation is used to smooth the images to allow larger motions (Adelson, Anderson, Bergen, Burt, & Ogden, 1984). The algorithm implemented in the present software package is based on the approach proposed by Lee et al. (2008) (hereinafter referred to as Lee's algorithm). The user needs to initialize the feature that will be tracked (Figure 2). This is done by selecting a window on this feature. The horizontal and vertical velocities of each pixel within the window (u and v, respectively) are then sorted separately in ascending order. In each ordered list, a specific number of pixels is discarded, both at the beginning and at the end of the list, since these extreme values of the velocities can differ from the others thereby damaging the tracking performance (Lee et al., 2008). The exclusion of these pixels helps to justify one of the OF assumptions, namely having similar pixel motion within the tracking window. By considering the remaining pixels, the means of the velocities of the first and last five pixels are calculated. Between these two means, the one with the greatest magnitude is added to the initial pixel position (x as horizontal, y as vertical) to obtain the new pixel position ($x + u$, $y + v$) in the following image. The window is then centred on the new feature position. Beside the method of Lee described above, a novel adaptation of the algorithm is proposed. According to this method the pixels within the window

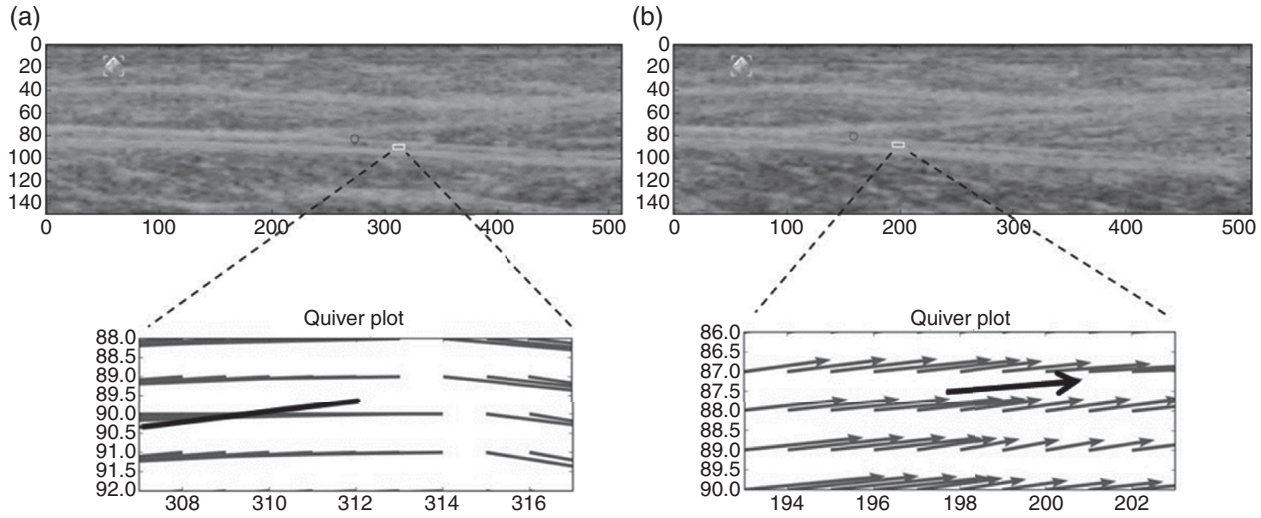

FIGURE 2 (a,b) Top: two US images cropped around the MTJ that are a representative example of a TD child during a fast movement. The pixel coordinates are depicted on the axes. The circle is the feature tracked whilst the rectangle represents the window where the algorithm is calculated. Bottom: the direction and magnitude of the single pixel velocities (grey) and resulting pixel velocity and direction computed by the algorithm (black). The pixel coordinates are depicted on the axes in accordance with the US image above. (a) An image with different direction and magnitude for the single pixel velocities. (b) An image with similar pixel behaviour

are divided into two groups according to the sign of their velocities. Two mean velocities are then calculated for each group. The mean velocity with positive sign is chosen depending on whether in the window a predominant positive sign for the velocities is found, whilst the negative sign is chosen with a predominant negative sign.

The software also allows one to include an offset between the feature of interest and the actual tracked point, such as between the location of the deep muscle aponeurosis (AP) and of the MTJ. This option can be a convenient tool for tracking other features in the image that are expected to rigidly move with the original feature of interest, but which are not easily trackable (Figure 2).

The software package allows tuning of the threshold for determining the number of pixels to be discarded for the tracking, as well as the number of pixels involved for moving the relevant feature. The implementation of the OF using the pyramid representation (Adelson et al., 1984) is performed using OpenCV wrapping for python. The window size is defined as 15×15, with two pyramid levels.

An additional feature of the software is the visualization of the magnitude and the direction of the velocities within the relevant window (Figure 2), as well as the definition of the profile of the velocity in the u and v directions (Figure 3). The mean and standard deviations of these velocities are also recorded for the whole sequence of images. Finally, a video made from this sequence of images with the automatically tracked feature superimposed can be saved (Supporting information).

2.5 | The semi-automatic tracking by manual intervention for tracking adjustments

In accordance with the criteria of the OF Lukas–Kanade method and Lee's algorithm (Lee et al., 2008), neighbouring pixels should have similar motion. Therefore, a quality measurement based on this concept has been introduced. The standard deviation (related to all the pixel velocities within the tracking window) can be displayed for each analysed image (Figure 4). This provides information to guide the MTJ tracking adjustment. A threshold for this standard deviation can be set and the processing will stop once the standard deviation is exceeded, prompting the user to manually define the MTJ feature. In this semi-automatic approach, coordinates for the MTJ can also be manually inserted in the corresponding script and the tracking is then forced to pass through these manually predefined coordinates during processing. This is particularly useful when the operator is aware of images crucial for the entire processing, such as the start of a gait cycle. These coordinate insertions can also be supported by watching a video of the corresponding automatic tracking in which the images responsible for triggering the tracking error can be checked.

2.6 | Guidelines for using the software (Figure 5)

(1) Dicom file: upload a dicom file containing a sequence of US images (uncompressed 2D DICOM files).

(2) Data cut: f1 and f2 refer to initial and final frame to be processed; *x*,*y* to crop the images horizontally and vertically, respectively.

(3) Initial condition: size of the tracking window (width and height); window centre is meant for defining where to place the window for computing the tracking, while MTJ offset is for defining the feature where the results will be expressed.

(4) Tracking: tick the box if you want to plot the images while tracking, and if you want to perform a manual adjustment (if so, define the relevant threshold). In addition, decide the algorithm to be used and the velocity bands exclusion/inclusion (expressed as a percentage).

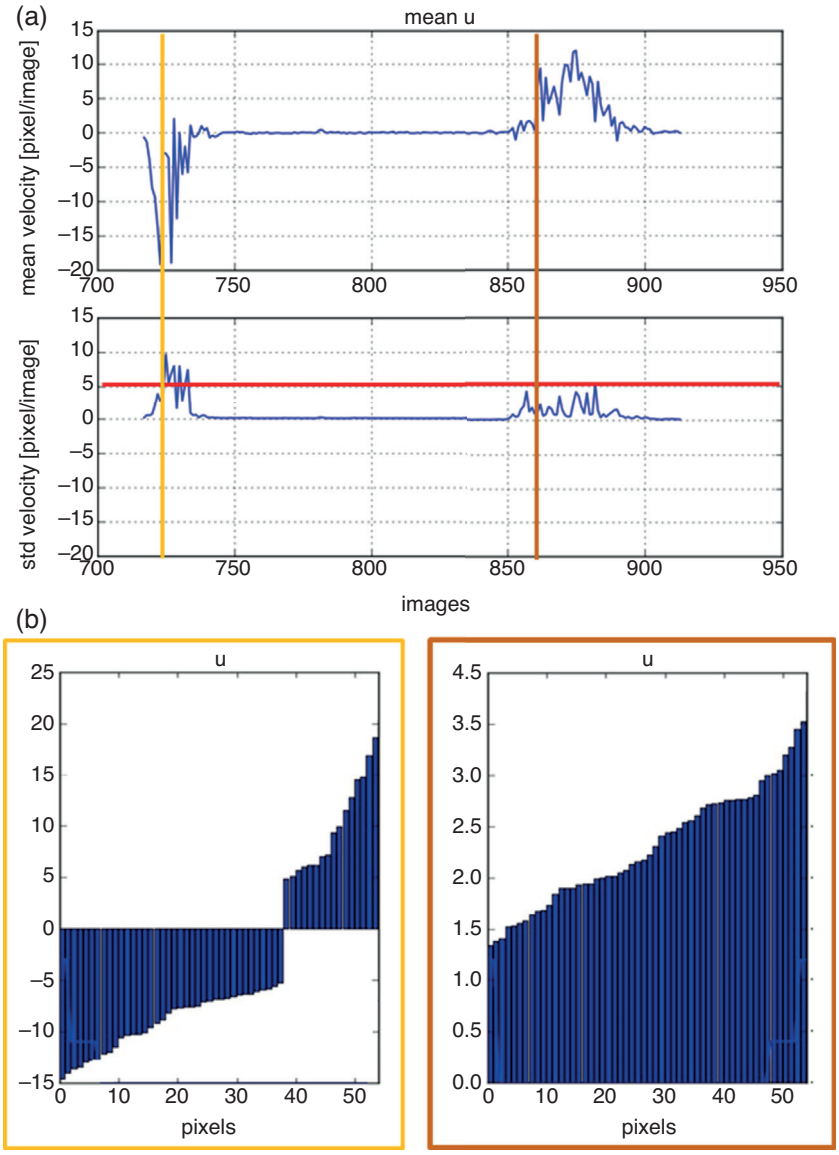

FIGURE 3 (a) Mean (avg) and the standard deviation (std) for the horizontal (u) pixel velocities computed by the algorithm, for all the images in the trial. The vertical lines indicate the particular image highlighted in the section below, whilst the horizontal line indicates a threshold for the standard deviations of the pixel velocities. (b) Velocity profile for the horizontal (*u*) pixel velocities for two representative images (the corresponding ones indicated as vertical line above)

(5) Results: decide if the intermediate data are needed and, if so, also the corresponding folder for saving such data, with thresholds as references; final data are saved as video (avi) and text file (res).

2.7 | Parameters selection

Images collected during slow and fast passive ankle rotations from a subgroup of eight children (4 TD and 4 with SCP: 2 GMFCS level I and 2 level II) were explored in a preliminary analysis to identify a suitable combination of tracking parameters. The following parameters were analysed: window location (MTJ, deep and superficial aponeurosis), windows size ((*u*,*v*): 11 × 5 and 77 × 35 pixels region), criteria for excluding the velocities (2 and 10 pixels) and criteria for computing the direction of the velocity (as described above). In addition, for the window location a perturbation of 5 pixels around the selected feature was applied, testing the possible manual error in initializing the tracking. The parameters that achieved the best results for the slow stretch were then applied for the fast stretch.

2.8 | Validation analysis

Based upon the above parameter selection study, a suitable combination of parameters was chosen. This parameter selection did not use fixed values for the criteria excluding the velocities (2, 6 and 10 pixels are the values utilized). The validation study was applied on the remaining larger population (8 TD; 8 children with SCP: 4 GMFCS level I and 4 level II; 8 TD adults). An experienced operator manually digitized the MTJ location for all the analysed participants to create the reference dataset. The automatic and the manual tracking results were compared using the root mean square errors (RMSE) and the corresponding absolute value of the MTJ excursion discrepancies. For the fast stretch, the results obtained with the semi-automatic tracking, i.e. adjusted with the guided manual intervention when needed, were also reported. For the walking trials, the following conditions were reported: (1) automatic tracking with one initialization, (2) semi-automatic tracking, which included adjustments with the guided manual intervention, (3) automatic tracking with the

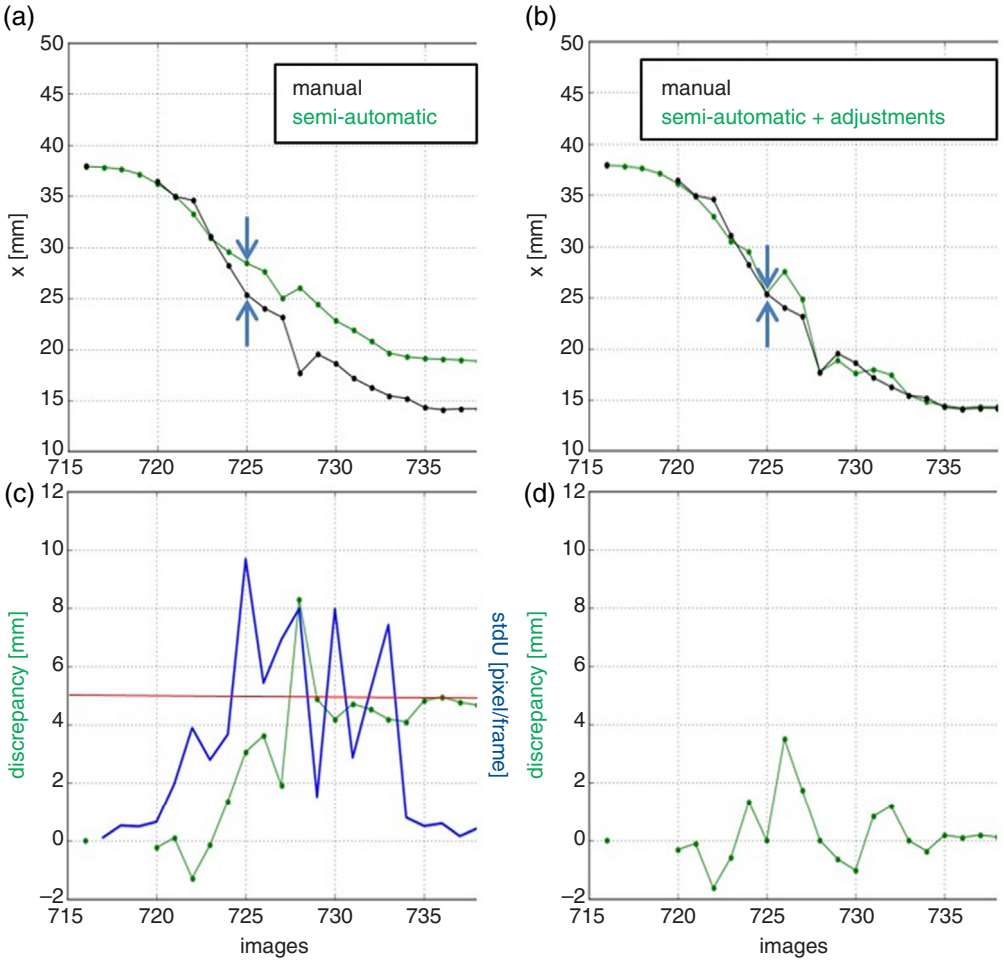

FIGURE 4 Example case of the tracking results (*x*, horizontally) with the manual (black) and the semi-automated method (green), before (a) and after (b) the application of the manual adjustments. The arrows indicated the reduction of the discrepancy in a specific image. (c) In blue the standard deviation of the velocity and in green the discrepancy of the automated method with respect to the manual one. The red line sets a 5 pixel/image threshold for the standard deviation. (d) In green the discrepancy of the adjusted method with respect to the manual one. The axis with images is cropped to emphasize the different variables during the movement

initializations at the beginning of each gait cycle, and (4) a combination of condition (2) and (3). The number of manual interventions was also reported. In addition, the manual tracking was performed two times to check the variability introduced by the operator.

3 | RESULTS

3.1 | Analysis on parameters selection for automatic tracking

By using a selection of the relevant tracking parameters, (1) the RMSE between the automatic tracking and the corresponding manual results, (2) the amount of excursion for the automatic MTJ tracking, and (3) the mean and absolute discrepancy between the automatic and manual tracking are shown in Table 1. A good compromise of the tracking parameters was found when the tracking window was situated on the deep AP, around 5–10 mm proximal with respect to the MTJ, and by choosing the novel criteria for the velocity direction (v1). On average, this corresponded to a slow stretch RMSE below 2.8 mm and an absolute discrepancy below 2.2 mm (Table 1). The fast stretch RMSE values were below 4.6 and 3.4 mm, respectively. Comparable RMSE and discrepancies values were found when using the different windows sizes. Small perturbations around the optimal window location revealed similar results with respect to the selected feature, with a tendency for worse results with the window slightly inside the muscle. Hence, for the subsequent validation analysis, the tracking window was placed on the deep AP, with the small window size and using the novel criteria for choosing the velocity direction. A threshold for excluding the velocities of 2 pixels was chosen.

3.2 | Validation of the automatic MTJ tracking during slow/fast velocity movements

A suitable combination of parameters found above was then used to apply the automatic tracking method to the larger cohorts of TD children and children with SCP. On average, 370 images were processed for the slow velocity and 296 for the fast velocity, requiring

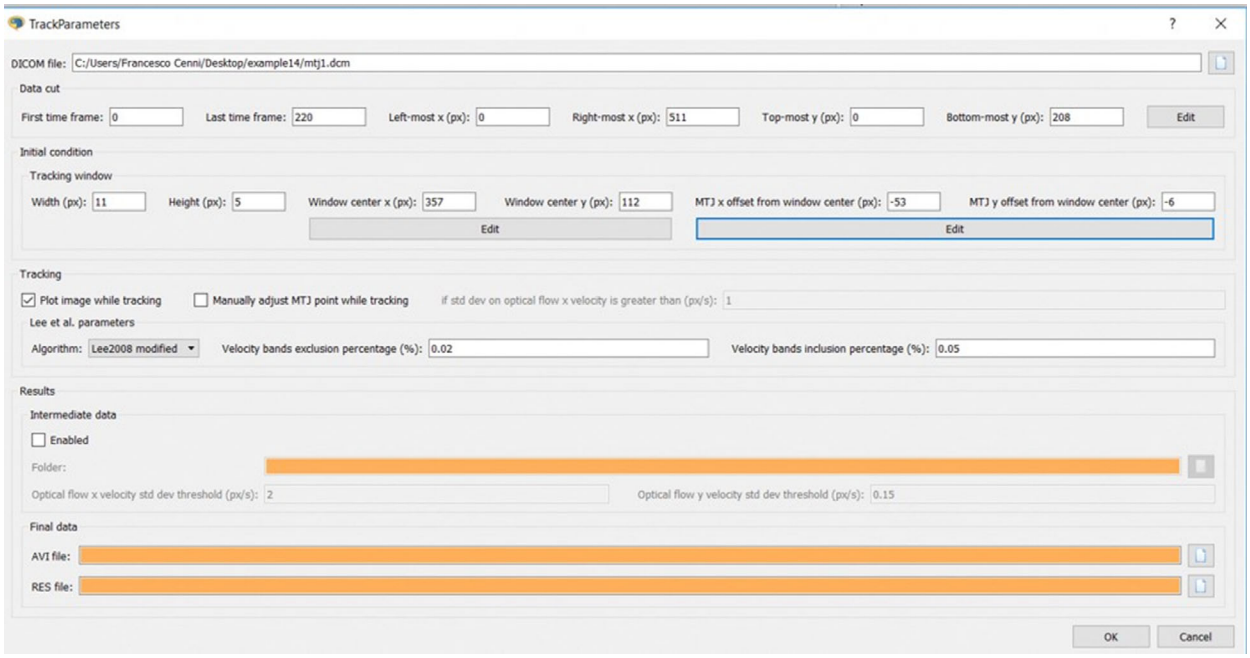

FIGURE 5 Snapshot of the GUI

a processing time of approximately 20 s for the whole sequence (on a 16 GB RAM Intel i7 2.7 GHz machine). The results of these analyses are reported in Tables 2 and 3. For the slow stretch, the RMSE values were lower than 3.1 mm (SCP cohort, GMFCS II) and the absolute discrepancies lower than 1.9 mm (TD cohort). Overall, with respect to the slow movement, higher RMSE and discrepancies were found for the fast movements (Table 3), particularly for the SCP group, being 5.2 mm and 4.9 mm, respectively. For the fast stretch, the data were further processed with different thresholds (6 and 10 pixels) for discarding the pixel velocities (Table 4). The criteria with a high threshold (10 pixels) provided better results for the SCP cohort for fast velocity movements.

3.3 | The semi-automatic tracking by manual adjustments according to the quality measurement

The results obtained from cohorts of SCP and TD children during fast movements (Table 3) were manually adjusted in accordance with the standard deviation of the velocities as a quality measurement. For this standard deviation a threshold of 5 pixels/image was set (Figure 3). This corresponded to manually inserting on average 5 points throughout the whole trial, adding approximately 1 min to the previously indicated processing time. Reductions of about 30% for the RMSE and absolute discrepancy compared with the automatic method were found (Table 3, Figure 4).

3.4 | Validation of MTJ tracking during walking

The automatic and semi-automatic tracking methods were applied to a cohort of healthy adults during walking. A total of 200 images were processed corresponding to a minimum of five gait cycles per participant. The RMSE decreased from 6.3 mm using the automatic method to 3.6 mm using semi-automatic approach with manual adjustments and initialization per gait cycle. Similar results were found in terms of absolute discrepancy. A considerable reduction in time was achieved with respect to the manual tracking method (Table 5).

4 | DISCUSSION

Calculating the displacement of the junction between a muscle and the tendon during joint movement can provide a deeper understanding of altered tissue behaviour to improve clinical decision making (Barber, Barrett, & Lichtwark, 2012; Kalsi et al., 2016). This has been mostly applied in sequences of US images to the MG MTJ. Although some attempts were made to put forward an automatic procedure (Lee et al., 2008; Pearson et al., 2013), the MG MTJ has commonly been manually extracted by relying on operator experience. This has especially occurred for identifying the MTJ in impaired muscles where visualization is often challenging due to the hyper-echoic muscle (Pitcher et al., 2015). The present study evaluates advances for an automatic procedure by providing an open-source software library, a validation analysis both in TD and in impaired muscles, and methodological tools for improving semi-automatic tracking outcomes. The tracking procedure was tested in the passive condition when moving the ankle joint at two velocities and in an active condition by walking on a treadmill. The decision to analyse these conditions as well as normal and impaired muscles was made to cover a large spectrum of possible acquisition set-ups, thus providing relevant results for the comparisons. These results can be used to decide whether this tracking procedure is suitable for further specific applications.

TABLE 1 Parameters selection

	RMSE (mm)	MTJ excursion automatic (mm)	Discrepancy (mm)	Absolute discrepancy (mm)
Slow stretch				
MTJ SW10	5.6 ± 3.5	18.2 ± 8.2	−7.0 ± 5.4	7.0 ± 5.4
MTJ SW2	5.6 ± 3.2	21.1 ± 9.8	−4.1 ± 7.4	6.5 ± 7.4
MTJ BW10	4.8 ± 3.0	19.9 ± 6.6	−5.3 ± 5.4	5.4 ± 5.4
MTJ BW2	4.7 ± 2.6	28.4 ± 5.9	3.3 ± 6.2	5.8 ± 6.2
deepAP_SW10	2.9 ± 1.7	22.5 ± 6.7	−2.6 ± 2.5	2.7 ± 2.5
supAP_SW10	13.2 ± 3.7	4.6 ± 2.8	−20.5 ± 5.6	20.5 ± 5.6
deepAP_SW2	2.7 ± 1.6	23.8 ± 7.1	−1.3 ± 2.2	1.9 ± 2.2
supAP_SW2	12.4 ± 3.0	5.6 ± 3.6	−19.6 ± 4.6	19.6 ± 4.6
deepAP_BW2	2.3 ± 1.3	24.4 ± 6.3	−0.7 ± 1.9	1.7 ± 1.9
deepAP_SW10_v1	2.7 ± 1.3	22.9 ± 6.2	−1.8 ± 2.1	2.1 ± 2.1
deepAP_SW2_v1	2.8 ± 1.2	25.8 ± 6.7	1.1 ± 2.4	2.2 ± 2.4
per1_deepAP_SW10_v1	2.7 ± 1.4	22.8 ± 6.5	−1.8 ± 1.9	2.1 ± 1.9
per2_deepAP_SW10_v1	2.5 ± 1.2	22.3 ± 7.1	−2.4 ± 2.2	2.4 ± 2.2
per3_deepAP_SW10_v1	3.4 ± 1.5	23.6 ± 7.2	−1.1 ± 3.2	2.8 ± 3.2
per4_deepAP_SW10_v1	3.4 ± 1.7	23.8 ± 7.0	−0.9 ± 3.0	2.5 ± 3.0
dist_deepAP_SW10_v1	2.7 ± 1.6	24.4 ± 5.7	−0.3 ± 2.7	2.1 ± 2.7
prox_deepAP_SW10_v1	2.7 ± 1.5	24.2 ± 6.9	−0.5 ± 3.1	2.4 ± 3.1
fast stretch				
deepAP_SW10	5.4 ± 2.6	20.7 ± 7.1	−4.2 ± 3.1	4.2 ± 3.1
deepAP_SW2	4.8 ± 2.5	21.9 ± 5.5	−2.9 ± 4.6	4.7 ± 4.6
deepAP_SW10_v1	5.4 ± 2.6	21.3 ± 6.5	−3.5 ± 3.7	4.2 ± 3.7
deepAP_SW2_v1	4.6 ± 2.2	22.2 ± 6.5	−2.7 ± 3.6	3.4 ± 3.6

The means and standard deviations of the following variables are reported: the root mean square errors (RMSE) between the semi-automatic tracking and the corresponding manual results, the amount of excursion for the muscle tendon junction (MTJ) tracked automatically, the discrepancy between the automatic and manual tracking, and the absolute discrepancy between the automatic and manual tracking. The following tests for the semi-automatic tracking methods are reported. The windows are located on the MTJ, deep and superficial (sup) aponeuroisis (AP). The size for small (SW) and big (BW) window are in pixels (11,5) and (77,35), respectively (approximately 1 pixel corresponds to 0.1 mm). Numbers 2 and 10 are related with the criteria for excluding the velocities within the algorithm, 2 and 10 pixels, respectively. v1 indicates the criteria for computing the direction of the velocity here proposed, whilst if no indicated, a previous methods was used (Lee et al., 2008). Some perturbations (per) were also applied in pixels (*x*,*y*): 1: (5,5), 2: (−5,5), 3: (−5,−5), 4: (5,−5). In addition, the window on the deep AP was moved distally (dist) and proximally (prox) with respect to the MTJ.

TABLE 2 Cohorts of children with spastic cerebral palsy (SCP) and typically developed (TD) performing a slow stretch

Participants	RMSE (mm)	MTJ excursion automatic (mm)	MTJ excursion manual (mm)	Absolute discrepancy (mm)
SCP (GMFCS I)	1.9 ± 0.9	16.9 ± 5.4	17.5 ± 6.3	1.3 ± 1.4
SCP (GMFCS II)	3.1 ± 2.0	21.2 ± 5.3	19.6 ± 5.4	1.6 ± 1.2
All SCP	2.5 ± 1.6	19.1 ± 5.5	18.6 ± 5.7	1.4 ± 1.2
TD	2.3 ± 1.1	29.3 ± 2.7	29.3 ± 3.0	1.9 ± 1.8

The SCP cohort is divided in two groups according to their GMFCS scores. Mean and standard deviation of the root mean square errors (RMSE), the muscle tendon junction (MTJ) automatically (auto) and manually tracked, and the corresponding absolute differences. The threshold used for discarding the pixel velocities is 2.

The first aim of the paper was to provide an open-source software library to apply the MTJ automatic tracking, based on Lee's algorithm as well as the semi-automatic tracking. The library is able to process sequences of images from any US device in a DICOM format, offering the possibility to tune the algorithm parameters through a graphical user interface (see Guidelines for using the software). The tracking adjustment is also supported by the library both during and prior to processing. The former is applied by requesting the operator to

TABLE 3 Cohorts of children with spastic cerebral palsy (SCP) and typically developed (TD) performing a fast stretch

	RMSE (mm)		MTJ excursion (mm)			Absolute discrepancy (mm)	
Participants	Automatic	Adjusted	Automatic	Adjusted	Manual	Automatic	Adjusted
SCP (GMFCS I)	5.9 ± 1.9	3.9 ± 1.7	17.2 ± 4.2	17.3 ± 5.6	16.2 ± 6.1	7.2 ± 3.7	4.4 ± 2.1
SCP (GMFCS II)	4.6 ± 1.7	3.0 ± 0.9	18.1 ± 0.9	16.3 ± 3.1	15.9 ± 3.1	2.6 ± 1.9	0.4 ± 0.3
All SCP	5.2 ± 1.8	3.4 ± 1.3	17.6 ± 2.8	16.8 ± 4.2	16.1 ± 4.5	4.9 ± 3.7	2.4 ± 2.6
TD	3.5 ± 2.3	2.6 ± 1.2	26.8 ± 5.1	27.3 ± 1.6	27.0 ± 4.3	2.5 ± 2.7	3.1 ± 1.5

The SCP cohort is divided into two groups according to their GMFCS scores. Mean and standard deviation of the root mean square errors (RMSE), the muscle tendon junction (MTJ) automatically, adjusted and manually tracked, and the corresponding absolute differences are reported. The threshold used for discarding the pixel velocities is 2.

TABLE 4 Cohorts of children with spastic cerebral palsy (SCP) and typically developed (TD) performing a slow and fast stretch

	6 pixels		10 pixels	
Participants (automatic tracking)	RMSE (mm)	Absolute discrepancy (mm)	RMSE (mm)	Absolute discrepancy (mm)
SCP	4.7 ± 2.3	2.7 ± 1.7	4.1 ± 2.5	3.2 ± 2.0
TD	2.8 ± 1.4	3.2 ± 2.0	4.2 ± 1.9	4.3 ± 2.5

Mean and standard deviation of the root mean square errors (RMSE), and for the absolute differences between the automatically and manually tracked are reported. The number of pixels to discard and the window size is indicated.

TABLE 5 Cohorts of healthy adults walking on a treadmill

Tracking method	RMSE (mm)	MTJ excursion (mm)	Absolute discrepancy (mm)	Time (min)
Automatic (only one initialization)	6.3 ± 4.0	19.3 ± 7.1	4.9 ± 5.6	~0.2
Automatic with manual adjustments	4.7 ± 2.0	17.6 ± 3.4	3.4 ± 2.5	~1
Automatic (with one initialization per gait cycle)	3.8 ± 1.5	18.7 ± 6.3	4.4 ± 3.1	~1
Manual adjustments and initialization per gait cycle	3.6 ± 1.7	18.6 ± 7.3	4.5 ± 3.6	~2
Manual repetition	1.7 ± 0.7	15.5 ± 3.9	1.0 ± 0.7	~20

Mean and standard deviation of the root mean square errors (RMSE), the muscle tendon junction (MTJ) excursion, the corresponding absolute differences with respect the manual tracking and time needed are reported. The threshold used for discarding the pixel velocities is 10.

manually digitize the MTJs in specific images. This is highlighted with a pop-up window during processing as potential failures of the algorithm, in accordance with the defined threshold of the standard deviation of the pixel velocities. This is a novel and efficient method to guide the operator in correcting the critical images during the automatic tracking process. Alternatively, before processing, specific image numbers along with the corresponding coordinates of the MTJ can be manually added, thereby forcing the tracking to go through these predefined coordinates. Finally, this library is a part of a more comprehensive software platform offering tools for experimental set-ups that combine ultrasonography and optical motion-tracking devices (Cenni et al., 2016). This combination can be exploited for several usages, such as estimating the actual length of muscle and tendon during joint movement, and not only their relative displacement (Kalsi et al., 2016).

Before validating the automatic algorithm, the most critical parameters of the tracking method were analysed in order to find a suitable combination. Lee's algorithm was modified by way of choosing the direction of the velocity to the next image. This is defined by the dominant number of velocities concordant in sign within the whole window, and not based on their magnitude in specific pixels (Lee et al., 2008). This offers more stable tracking, in particular when peaks caused by artefacts in the pixel velocities profile wrongly move the relevant feature. Due to the satisfactory results for both slow and fast stretch (Table 1), this modified selection of velocities was chosen. Another important parameter was the location of the tracking window. Improvements of at least 50% for the RMSE and for the absolute discrepancy were found when the tracking window was placed 5–10 mm proximal to the MTJ, thus including the MG's deep AP instead of selecting directly the MTJ (Table 1). This probably occurred for a number of reasons. During joint movement, the MTJ appears to be a less consistent image feature as the 'V' shape of the MTJ often moves out of the image plane, making it more challenging to consistently distinguish. In addition, the effects of deformation appeared more around the MTJ than at the deep AP. However, the outcome still refers to the MTJ displacement, since an offset between the MTJ and the actual tracked point is used. A possible manual error for testing the tracking initialization was evaluated by adding 5 pixels of perturbation around the original feature. While this does not seem to damage the outcome, caution should be taken not to place the window on the border between the deep AP and the internal section of the muscle (Table 1). With respect to the size of the tracking window, similar results were found. To simplify the computation, a small size was chosen (11 × 5 pixels). Finally, Lee's algorithm proposed 10 pixels as thresholds for excluding the pixel velocities. The analysis for the parameters selection suggested better results using 2 pixels as thresholds.

The second aim of the paper was to validate the automatic tracking algorithm during passive and active ankle movements using the aforementioned parameterization. The passive movement analysis

revealed satisfactory results for the slow stretch applied in the TD cohort, with 7% difference between the manual and automated tracking (Table 2). This is in line with a preliminary investigation using a similar approach (Lee et al., 2008). Interestingly, the SCP group had similar absolute results to the TD group (about 2 mm), although higher as a percentage due to the smaller range of motion achieved by these children. Nevertheless, previous repeatability analyses by means of manual tracking reported MTJ variability within 1–2 mm, which is not an easily identifiable point feature (Ito et al., 2000). MTJ identification becomes even more challenging in hyper-echoic muscles (Cenni et al., 2018). As expected, an increase of the RMSE/absolute discrepancy was found in the more involved SCP GMFCS II group, which may be due to their hyper-echoic appearance (Pitcher et al., 2015).

The fast stretch data (a 5.5 Hz average frequency from plantar- to dorsiflexion) were analysed as possible critical scenarios for the automatic tracking method, due to the large and dissimilar pixel motion between images. Overall, the fast movement results for the TD cohort were quite comparable to those obtained during a slow movement, whilst for the children with SCP the fast movement errors were quite large, i.e. 5.2 and 4.9 mm for RMSE and discrepancy, respectively. In the SCP cohort, a recoil of the muscle was observed during the fast movement, moving the tracking window away from the relevant feature and introducing a bias in the final outcome. This behaviour is known to occur in children with SCP due to hyper-excitability of the MG and surrounding muscles in response to fast velocity stretch, possibly deforming the muscle structures at the time of the movement reflex (Bar-On et al., 2018). The automatic tracking method was not satisfactory for the data acquired on the treadmill, with on average a discrepancy of 6.3 mm for the RMSE.

The third aim of the paper was to develop a semi-automatic tracking approach, by introducing a tool for guiding manual intervention. This tool aimed to improve the MTJ tracking based on the standard deviation of the velocity within the tracking window. High values for the standard deviation were found when MTJ mal-tracking occurred (Figures 3 and 4). This is based on the assumption that OF works properly when, within the tracking window, the pixels move approximately with the same magnitude in the same direction. In the present investigation, this assumption was not entirely satisfied for large feature movements between two consecutive images. This was especially the case when the joint movement was fast and elicited a stretch reflex in SCP muscles. In this specific condition, the manual adjustment enabled reduced tracking errors with values in line with the TD cohort (Table 4). Obviously, the smaller the threshold, the better the results. The decision on the threshold is a trade-off between the time available for a manual intervention and the quality of the tracking results. In the case of a different US device, type of movements and muscle pathology, a different threshold will probably be needed. The advantage of adjusting the automatic tracking method was also present for the walking trials. For these trials, a combination of adjustments prior to and during the tracking were performed, revealing an improvement for the RMSE of about 50%. Adjustment prior to the tracking is a suitable solution for MTJ cycle displacements, such as during walking.

There are a number of limitations in the present investigation. The initialization is manually performed, and thus different window placement could affect the outcomes. To limit such outcome variability, the window placements were analysed in the parameter section and relevant guidelines are provided. The parameter selection showed promising results, within 2–3 mm for RMSE and absolute discrepancy, and thus suitable for several applications. However, in order to find an optimal set of parameters, further explorations can optimize the parameters for the particular implementation at hand. For the validation analysis, the reference data were obtained by a manual tracking with intrinsic errors. This introduced a subjective factor in this analysis, which becomes more relevant with impaired muscles, since it is more challenging to identify the MTJ. Therefore, multiple manual MTJ extractions should be performed and the corresponding variability used as a reference. However, the comparison with one manual repetition is still relevant, since it allows an assessment of whether the automated method is in line with the commonly applied manual digitization. In addition, a second manual repetition was performed for walking trials. The results also depend on the US image quality. Hence, the use of a higher-quality US device may potentially lead to different results. For the present analysis, the US settings during the acquisition were optimized for each child to allow the best MTJ visibility. It may occur that during the ankle motion the MTJ moves slightly out of the image plane. This can damage the tracking method. However, this does not often occur and the semi-automatic method can limit the consequential errors. The results obtained can also vary according to the frequency used for recording US images. For the slow movement, a frequency of 30 Hz does not seem to be an issue. For the fast movement, 60 Hz was defined as a good compromise with image quality. For a similar movement, a higher frequency (e.g. 80 Hz) would further reduce the change in pixel distance between consecutive images. This could improve the correlation of the local environment of pixels between these consecutive images, together with the automatic tracking. This however depends on the US device, since higher sampling frequency can increase image noise.

5 | CONCLUSION

This investigation provided an open-source library capable of tracking the MTJ following an automatic as well as a semi-automatic approach. This library was validated during passive and active ankle joint movements. Typically developing muscles and muscles of children with SCP were analysed providing satisfactory results. Tracking errors increased in the walking condition and in hyper-echoic muscles, the latter occurring in children with SCP. Critical images that lead to poor automatic tracking performances were identified and communicated to the operator, who, in turn, can adjust the outcome. The final semi-automatic method seems applicable in other neuromuscular pathologies. To increase the reproducibility of this research, the developed software package is made available at https://gitlab.com/u0078867/py3dfreehandus.

COMPETING INTERESTS

The authors declare that we have no financial or personal relationships with other people or organizations that could inappropriately influence (bias) our work.

AUTHOR CONTRIBUTIONS

F.C., D.M., E.A., K.D. and H.B. were involved in the conception of this research investigation, whilst F.C., L.B., S.H.S. and B.K. were involved in the data acquisition and analysis. All authors had complete access to the study data that support the publication, were involved in the drafting or critical revisions of the manuscript and approved the final version of the manuscript. In addition, all authors agree to be accountable for all aspects of the work in ensuring that questions related to the accuracy or integrity of any part of the work are appropriately investigated and resolved. All persons designated as authors qualify for authorship, and all those who qualify for authorship are listed.

ORCID

Francesco Cenni https://orcid.org/0000-0001-8637-8853

REFERENCES

Adelson, E. H., Anderson, C. H., Bergen, J. R., Burt, P. J., & Ogden, J. M. (1984). Pyramid methods in image processing. *RCA Engineer*, *29*, 33–41.

Barber, L., Barrett, R., & Lichtwark, G. (2012). Medial gastrocnemius muscle fascicle active torque-length and Achilles tendon properties in young adults with spastic cerebral palsy. *Journal of Biomechanical Engineering*, *45*, 2526–2530. https://doi.org/10.1016/j.jbiomech.2012.07.018.

Barber, L., Carty, C., Modenese, L., Walsh, J., Boyd, R., & Lichtwark, G. (2017). Medial gastrocnemius and soleus muscle-tendon unit, fascicle, and tendon interaction during walking in children with cerebral palsy. *Developmental Medicine and Child Neurology*, *59*, 843–851. https://doi.org/10.1111/dmcn.13427.

Bar-On, L., Aertbeliën, E., Wambacq, H., Severijns, D., Lambrecht, K., Dan, B., … Desloovere, K. (2013). A clinical measurement to quantify spasticity in children with cerebral palsy by integration of multidimensional signals. *Gait & Posture*, *38*, 141–147. https://doi.org/10.1016/j.gaitpost.2012.11.003.

Bar-On, L., Kalkman, B. M., Cenni, F., Schless, S. H., Molenaers, G., Maganaris, C. N., … Desloovere, K. (2018). The relationship between medial gastrocnemius lengthening properties and stretch reflexes in cerebral palsy. *Frontiers in Pediatrics*, *6*, 259. https://doi.org/10.3389/fped.2018.00259.

Bénard, M. R., Becher, J. G., Harlaar, J., Huijing, P., & Jaspers, R. T. (2009). Anatomical information is needed in ultrasound imaging of muscle to avoid potentially substantial errors in measurement of muscle geometry. *Muscle & Nerve*, *39*, 652–665. https://doi.org/10.1002/mus.21287.

Cenni, F., Bar-On, L., Schless, S. H., Kalkman, B., Aertbeliën, E., Bruyninckx, H., & Desloovere, K. (2018). Medial gastrocnemius muscle–tendon junction and fascicle lengthening across the range of motion analyzed in 2-D and 3-D ultrasound images. *Ultrasound in Medicine & Biology*, *44*, 2505–2518. https://doi.org/10.1016/j.ultrasmedbio.2018.07.012.

Cenni, F., Monari, D., Desloovere, K., Aertbeliën, E., Schless, S. H., & Bruyninckx, H. (2016). The reliability and validity of a clinical 3D freehand ultrasound system. *Computer Methods and Programs in Biomedicine*, *136*, 179–187. https://doi.org/10.1016/j.cmpb.2016.09.001.

Cronin, N. J., Carty, C. P., Barrett, R. S., & Lichtwark, G. (2011). Automatic tracking of medial gastrocnemius fascicle length during human locomotion. *Journal of Applied Physiology*, *111*, 1491–1496. https://doi.org/10.1152/japplphysiol.00530.2011.

Darby, J., Hodson-Tole, E. F., Costen, N., & Loram, I. D. (2012). Automated regional analysis of B-mode ultrasound images of skeletal muscle movement. *Journal of Applied Physiology*, *112*, 313–327. https://doi.org/10.1152/japplphysiol.00701.2011.

Darby, J., Li, B., Costen, N., Loram, I., & Hodson-tole, E. (2013). Estimating skeletal muscle fascicle curvature from b-mode ultrasound image sequences. *IEEE Transactions on Bio-medical Engineering*, *60*, 1935–1945. https://doi.org/10.1109/TBME.2013.2245328.

Ito, M., Akima, H., & Fukunaga, T. (2000). In vivo moment arm determination using B-mode ultrasonography. *Journal of Biomechanics*, *33*, 215–218. https://doi.org/10.1016/S0021-9290(99)00154-2.

Kalkman, B. M., Bar-On, L., Cenni, F., Maganaris, C. N., Bass, A., Holmes, G., … O'Brien, T. D. (2017). Achilles tendon moment arm length is smaller in children with cerebral palsy than in typically developing children. *Journal of Biomechanics*, *56*, 48–54. https://doi.org/10.1016/j.jbiomech.2017.02.027.

Kalsi, G., Fry, N. R., & Shortland, A. P. (2016). Gastrocnemius muscle–tendon interaction during walking in typically-developing adults and children, and in children with spastic cerebral palsy. *Journal of Biomechanics*, *49*, 3194–3199. https://doi.org/10.1016/j.jbiomech.2016.07.038.

Lee, S. S. M., Lewis, G. S., & Piazza, S. J. (2008). An algorithm for automated analysis of ultrasound images to measure tendon excursion in vivo. *Journal of Applied Biomechanics*, *24*, 75–82.

Lucas, B. D., & Kanade, T. (1981). An iterative image registration technique with an application to stereo vision. *Proceedings of the International Joint Conference Artificial Intelligence*, *130*, 674–679.

Maganaris, C. N. (2002). Tensile properties of in vivo human tendinous tissue. *Journal of Biomechanics*, *35*, 1019–1027.

Magnusson, S. P., Hansen, P., Aagaard, P., Brønd, J., Dyhre-Poulsen, P., Bojsen-Moller, J., & Kjaer, M. (2003). Differential strain patterns of the human gastrocnemius aponeurosis and free tendon, in vivo. *Acta Physiologica Scandinavica*, *177*, 185–195.

Obst, S. J., Boyd, R., Read, F., & Barber, L. (2017). Quantitative 3-D ultrasound of the medial gastrocnemius muscle in children with unilateral spastic cerebral palsy. *Ultrasound in Medicine & Biology*, *43*, 2814–2823. https://doi.org/10.1016/j.ultrasmedbio.2017.08.929.

Pearson, S. J., Ritchings, T., & Mohamed, A. S. A. (2013). The use of normalized cross-correlation analysis for automatic tendon excursion measurement in dynamic ultrasound imaging. *Journal of Applied Biomechanics*, *29*, 165–173. https://doi.org/10.1123/jab.29.2.165.

Pitcher, C. A., Elliott, C. M., Panizzolo, F. A., Valentine, J. P., Stannagem, K., & Reid, S. L. (2015). Ultrasound characterization of medial gastrocnemius tissue composition in children with spastic cerebral palsy. *Muscle & Nerve*, *52*, 397–403. https://doi.org/10.1002/mus.24549.

Rana, M., Hamarneh, G., & Wakeling, J. M. (2009). Automated tracking of muscle fascicle orientation in B-mode ultrasound images. *Journal of Biomechanics*, *42*, 2068–2073. https://doi.org/10.1016/j.jbiomech.2009.06.003.

Schless, S. H., Cenni, F., Bar-On, L., Hanssen, B., Kalkman, B., O'Brien, T., … Desloovere, K. (2018). Medial gastrocnemius volume and echointensity after botulinum neurotoxin A interventions in children with spastic cerebral palsy. *Developmental Medicine and Child Neurology*, *61*, 783–790. https://doi.org/10.1111/dmcn.14056.

Schless, S. H., Desloovere, K., Aertbeliën, E., Molenaers, G., Huenaerts, C., & Bar-On, L. (2015). The intra- and inter-rater reliability of an instrumented spasticity assessment in children with cerebral palsy. *PLoS One*, *10*, e0131011. https://doi.org/10.1371/journal.pone.0131011.

Sikdar, S., Wei, Q., & Cortes, N. (2014). Dynamic ultrasound imaging applications to quantify musculoskeletal function. *Exercise and Sport Sciences Reviews*, *42*, 126–135. https://doi.org/10.1249/JES.0000000000000015.

Theis, N., Mohagheghi, A. A., & Korff, T. (2016). Mechanical and material properties of the plantarflexor muscles and Achilles tendon in children with spastic cerebral palsy and typically developing children. *Journal of Biomechanics*, *49*, 3004–3008. https://doi.org/10.1016/j.jbiomech.2016.07.020.

Zhao, H., & Zhang, L. Q. (2011). Automatic tracking of muscle fascicles in ultrasound images using localized radon transform. *IEEE Transactions on Bio-medical Engineering*, *58*, 2094–2101. https://doi.org/10.1109/TBME.2011.2144593.

SUPPORTING INFORMATION

Additional supporting information may be found online in the Supporting Information section at the end of the article.

How to cite this article: Cenni F, Bar-On L, Monari D, et al. Semi-automatic methods for tracking the medial gastrocnemius muscle–tendon junction using ultrasound: a validation study. *Experimental Physiology*. 2019;1–12. https://doi.org/10.1113/EP088133